*Int. J. Heat Mass Transfer.* Vol. 36, No. 8, pp. 2027–2038, 1993
Printed in Great Britain

0017–9310/93 $6.00+0.00


# The resonance of natural convection in an enclosure heated periodically from the side

J. L. LAGE
Mechanical Engineering Department, Southern Methodist University, Dallas, TX 75275-0335, U.S.A.

and

A. BEJAN
Department of Mechanical Engineering and Materials Science, Box 90300, Duke University, Durham, NC 27708-0300, U.S.A.

(*Received* 27 *July* 1992 *and in final form* 27 *October* 1992)

**Abstract**—This is a numerical and theoretical investigation of natural convection in a two-dimensional square enclosure with one side cold and isothermal, and the other side heated with pulsating heat flux. It is shown numerically that the buoyancy induced circulation resonates to a certain (single) frequency of the pulsating heat input. The resonance is characterized by maximum fluctuations in the total heat transfer rate through the vertical midplane of the cavity. The numerical experiments cover the Prandtl number range 0.01–7, the heat flux Rayleigh number range $10^3$–$10^9$, and the nondimensional frequency range 0–0.3. It is shown that the critical frequencies determined numerically can be anticipated based on theoretical grounds, by matching the period of the pulsating heat input to the period of the rotation (circulation) of the enclosed fluid. In the last section, the same theoretical argument is used to predict the critical period for natural convection resonance in an enclosed porous medium saturated with fluid.

## 1. INTRODUCTION

THE WORK reported in this paper was motivated by a problem encountered in the design of experimental apparatuses for the study of natural convection in enclosed fluids. In most designs, one wall of the enclosure is cooled and another one heated, while the remaining walls are well insulated. When the objective is to study only the circulation and temperature distribution in the fluid, a simple and satisfactory technique is to control the temperatures of the differentially heated walls by means of two constant-temperature baths.

When the experiment is expected to deliver the heat transfer rate between two walls, in addition to the flow and fluid temperature, it is customary to heat the warm wall electrically while cooling the other wall with a constant temperature bath. The problem addressed in this paper is related to this second class of designs, in which the heat input must be controlled in order to control (i.e. increase or decrease) the temperature of the warm wall. A simple way of building this control capability into the design of the wall heating system is to use a set of electric resistances and to power them intermittently, with constant power during the 'on' mode, and less (or zero) power during the 'off' mode. The control of the temperature of the heated wall is achieved by varying the relative size of the time intervals associated with the on and off modes. On the right-hand side of Fig. 1, for example, higher values of the ratio $Z/(W-Z)$ lead to higher temperatures on the fluid surface of the heated wall.

A basic problem that is associated with the on/off heat input as a design feature is that the periodicity of the heating effect may alter in a substantial way the natural circulation and its heat transfer characteristics. This is not only a practical issue that needs to be addressed in the design of the apparatus, but a selfstanding fundamental problem in natural convection. That problem is to determine under what conditions the fluctuation of the heat input has a major influence on natural convection and heat transfer inside the enclosure. This fundamental question was already addressed in the realm of forced convection, where Zumbrunnen [1] showed that the fluid temperature and heat transfer capability may respond to the oscillation of the wall heat input.

There are several additional reasons, practical and theoretical, for investigating the natural convection resonance phenomenon in a fundamental way. On the practical side, in addition to the apparatus design problem mentioned already, there is the behavior of air spaces (e.g. rooms) and bodies of water (reservoirs, lakes) in which the recirculation is driven periodically by the daily solar flux. On the theoretical side, there is an emerging subfield in natural convection research that is concerned with the response of an enclosed fluid to time-dependent thermal boundary conditions [2–17]. For example, Patterson and Imberger [2] described the unsteady natural convection in an

## NOMENCLATURE

| | |
|---|---|
| $f$ | nondimensional frequency, equation (11) |
| $f_N$ | nondimensional $N$ frequency, $f_N \sim Ra^{-1/10}$ |
| $g$ | gravitational acceleration |
| $H$ | height |
| $k$ | fluid thermal conductivity |
| $k_m$ | thermal conductivity of saturated porous medium |
| $K$ | permeability |
| $L$ | length |
| $N$ | Brunt–Väisälä frequency, $(\beta g \Delta T/H)^{1/2}$ |
| $Nu_c$ | cold side Nusselt number, equation (13) |
| $Nu_h$ | hot side Nusselt number, equation (15) |
| $Nu_{loc}$ | local Nusselt number, equation (12) |
| $Nu_m$ | vertical midplane Nusselt number, equation (14) |
| $p$ | pressure |
| $P$ | nondimensional pressure |
| $Pr$ | Prandtl number |
| $q'_m$ | total heat transfer rate through the vertical midplane |
| $q''$ | heat flux |
| $\bar{q}'_c$ | heat flux averaged over the cold wall |
| $q''_M$ | mean heat flux value |
| $Q''$ | nondimensional heat flux, equation (9) |
| $Ra$ | flux Rayleigh number, equation (8) |
| $Ra_{\Delta T}$ | temperature difference Rayleigh number, equation (17) |
| $Ra_D$ | flux Rayleigh number for Darcy flow, equation (30) |
| $Ra_{D,\Delta T}$ | temperature difference Rayleigh number for Darcy flow, equation (29) |
| $Ra_F$ | flux Rayleigh number for Forchheimer flow, equation (36) |
| $Ra_{F,\Delta T}$ | temperature difference Rayleigh number for Forchheimer flow, equation (35) |
| $t$ | time |
| $T$ | temperature |
| $T_c$ | cold side temperature |
| $\bar{T}_h$ | average hot side temperature |
| $T_{ref}$ | reference temperature |
| $u, v$ | velocity components |
| $U, V$ | nondimensional velocity components |
| $w$ | period |
| $W$ | nondimensional period |
| $x, y$ | coordinates |
| $X, Y$ | nondimensional coordinates |
| $z$ | half period |
| $Z$ | nondimensional half period. |

Greek symbols

| | |
|---|---|
| $\alpha$ | fluid thermal diffusivity |
| $\alpha_m$ | thermal diffusivity of saturated porous medium |
| $\beta$ | coefficient of volumetric thermal expansion |
| $\theta$ | nondimensional temperature |
| $\theta_h$ | average nondimensional hot side temperature, equation (16) |
| $\nu$ | kinematic viscosity |
| $\rho$ | density |
| $\tau$ | nondimensional time |
| $\chi$ | quadratic term coefficient, equation (33) |
| $\psi$ | streamfunction. |

enclosure whose left and right wall temperatures are suddenly changed by $+\Delta T$ and $-\Delta T$, respectively. Nicolette *et al.* [8] investigated the approach to steady state in a rectangular enclosure in which the temperature of one side wall is changed suddenly to a new level, while the remaining walls are insulated.

Kazmierczak and Chinoda [16] documented numerically the steady periodic flow in a square

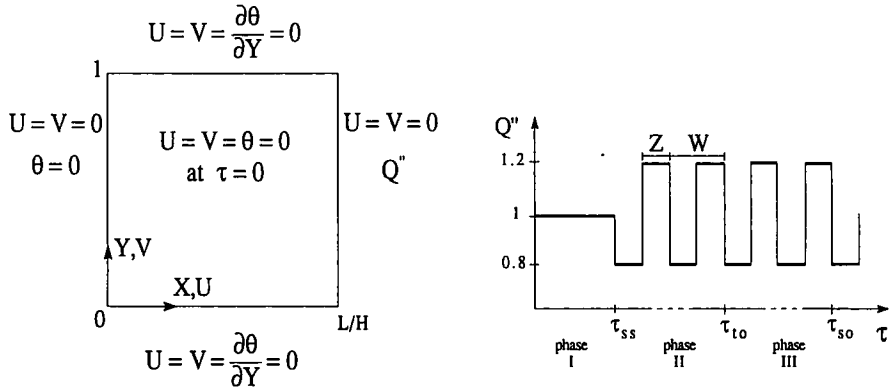


FIG. 1. Two-dimensional enclosure heated with pulsating heat flux from the right side.

enclosure with one side cold at constant temperature, and the other side at a higher temperature that is uniform along the wall (vertically) and varies sinusoidally in time. Their flow corresponds to 'phase III' of the time-dependent phenomenon considered in the present study (Fig. 1, right side), and is restricted to one Rayleigh number ($Ra_{\Delta T} = 1.4 \times 10^5$) and one Prandtl number ($Pr = 7$). Kazmierczak and Chinoda simulated flows for three different frequency settings for the fluctuation of the hot wall temperature, and showed that the frequency has an effect on the enclosure flow. Specifically, they reported a *monotonic* relationship between the period of wall temperature oscillation and the amplitude of the fluctuation exhibited by the mass flowrate of the gyre (fluid wheel) that turns inside the enclosure. In other words, they did not detect resonance between the wall temperature and flow oscillations.

The focus of the present paper is on the resonance between enclosed natural convection and pulsating wall heating. For this reason the study is based on a wide range of heat input frequencies, flux Rayleigh numbers $Ra$ ($10^3$–$10^9$) and Prandtl numbers (0.01–7). The work is a combination of empiricism and theory, namely numerical simulations accompanied by theoretical order-of-magnitude predictions (scale analysis).

## 2. MATHEMATICAL FORMULATION

The flow model is based on the assumptions that the fluid is Newtonian and that the properties are constant, with the exception of the density in the body force term of the momentum equation. The Oberbeck–Boussinesq [18, 19] approximation is used to relate density changes to temperature changes, and to couple in this way the temperature field to the flow field. The nondimensional equations for the conservation of mass, momentum and energy are written with reference to the left side of Fig. 1,

$$\frac{\partial U}{\partial X} + \frac{\partial V}{\partial Y} = 0 \tag{1}$$

$$\frac{DU}{D\tau} = -\frac{\partial P}{\partial X} + \left(\frac{Pr}{Ra}\right)^{1/2} \nabla^2 U \tag{2}$$

$$\frac{DV}{D\tau} = -\frac{\partial P}{\partial Y} + \left(\frac{Pr}{Ra}\right)^{1/2} \nabla^2 V + \theta \tag{3}$$

$$\frac{D\theta}{D\tau} = (Ra\,Pr)^{-1/2} \nabla^2 \theta \tag{4}$$

where $D/D\tau = \partial/\partial\tau + U\,\partial/\partial X + V\,\partial/\partial Y$, and $\nabla^2 = \partial^2/\partial X^2 + \partial^2/\partial Y^2$. The nondimensional variables are defined by

$$(X, Y) = \frac{(x, y)}{H}, \quad (U, V) = \frac{(u, v)}{(\alpha/H)(Ra\,Pr)^{1/2}} \tag{5}$$

$$\tau = \frac{\alpha t}{H^2}(Ra\,Pr)^{1/2}, \quad \theta = \frac{T - T_c}{q''_M H/k} \tag{6}$$

$$P = \frac{H^2(p + \rho g y)}{\rho \alpha^2\, Ra\, Pr}, \quad Pr = \frac{\nu}{\alpha} \tag{7}$$

$$Ra = \frac{g\beta q''_M H^4}{\alpha \nu k}. \tag{8}$$

The initial and boundary conditions for flow and temperature are indicated on the left side of Fig. 1. The cross-section of the two-dimensional cavity is square, $L/H = 1$, and the horizontal walls are insulated. The left side of the enclosure is isothermal and cold ($T = T_c$, or $\theta = 0$). The right side is heated with the heat flux $q''(t)$, which is distributed uniformly along the surface, and changes with time as shown on the right side of Fig. 1. The nondimensional heat flux function $Q''(\tau)$ is defined by

$$Q'' = \frac{q''}{q''_M} \tag{9}$$

where $q''_M$ is the mean value of the heat flux.

There are three distinct phases in the time dependent evolution of the flow and temperature in the fluid. In phase I, the fluid is warmed up to a steady state ($\tau \sim \tau_{ss}$) in which the circulation is driven by uniform flux ($q''_M$) from the right, and uniform temperature ($T_c$) from the left. This first phase is similar (but not identical) to the transient natural convection processes described in refs. [2, 8–10].

In phase II the heat flux fluctuates in square wave fashion about the mean value $q''_M$. The flow and temperature fields progress from the steady state reached at the end of phase I, toward a steady periodic (oscillatory) state marked by $\tau \sim \tau_{to}$. The amplitude of the heat flux wave is fixed at 20% of the mean value. In the present case, the dimensionless period of the heat flux wave is twice the time interval associated with peak heat flux, $W = 2Z$. According to the $\tau$ definition (6), these time intervals are defined by

$$(W, Z) = (w, z)(\alpha/H^2)(Ra\,Pr)^{1/2} \tag{10}$$

where $w$ is the actual period. The nondimensional frequency $f$ is defined by

$$W = 2Z = 1/f. \tag{11}$$

At times greater than $\tau_{to}$, the flow settles in the steady oscillatory state, or phase III.

To study the path followed by the total instantaneous heat input ($q' = q''H$) through the enclosure, it is helpful to document the behavior of the cold side local Nusselt number,

$$Nu_{loc} = \left.\frac{\partial \theta}{\partial X}\right|_{X=0} \tag{12}$$

the heat flux averaged over the cold wall ($\bar{q}''_c$), or the cold side overall Nusselt number,

$$Nu_c = \frac{\bar{q}''_c}{q''_M} = \int_0^1 \left.\frac{\partial \theta}{\partial X}\right|_{X=0} dY \tag{13}$$

and the instantaneous heat transfer rate through the

vertical midplane of the enclosure ($q'_m$), or the corresponding overall Nusselt number,

$$Nu_m = \frac{q'_m/H}{q''} = \int_0^1 \left[ (Ra\,Pr)^{1/2} U\theta - \frac{\partial\theta}{\partial X} \right]_{X=1/2} \mathrm{d}Y. \tag{14}$$

The overall Nusselt number for the hot side, or the instantaneous wall averaged temperature $\bar{T}_h$, can be calculated by writing

$$Nu_h = \frac{q''_M H}{(\bar{T}_h - T_c)k} = \frac{1}{\theta_h} \tag{15}$$

where

$$\theta_h = \int_0^1 \theta|_{X=1}\,\mathrm{d}Y. \tag{16}$$

The Rayleigh number based on the average instantaneous side-to-side temperature difference $(\bar{T}_h - T_c)$ is proportional to the heat flux Rayleigh number $Ra$ of equation (8),

$$Ra_{\Delta T} = \frac{g\beta(\bar{T}_h - T_c)H^3}{\alpha\nu} = \theta_h\, Ra. \tag{17}$$

## 3. NUMERICAL METHOD

The method chosen for the numerical simulations was the finite-differences control-volume method of Patankar [20]. It was chosen because of earlier experience with this method in problems of buoyancy induced flow and heat transfer (e.g. refs. [16, 21, 22]). The general features of our application of this method (algorithm, grid, tri-diagonal solver, etc.) are described in detail in ref. [22]. The convergence of the numerical results is established locally based on the criterion

$$\mathrm{MAX}\left| \frac{\phi^{i+1} - \phi^i}{\phi^i} \right| < 10^{-3} \tag{18}$$

where $\phi$ is replaced by $U$, $V$ and $\theta$ at every position $(X, Y)$ in the computational domain, and $i$ and $i+1$ are two consecutive iterations at the same time $\tau$. Accuracy tests showed that the solutions that satisfy the local criterion (18) exhibit a relative error smaller than $10^{-6}$ between two consecutive iterations on the overall Nusselt number.

Additional accuracy tests were performed to select a nonuniform grid of $82 \times 82$ nodes. The relative change exhibited by the overall Nusselt number is less than 2% when the grid changes from $62 \times 62$ nodes to $82 \times 82$ nodes. The chosen grid is finer than the $36 \times 45$ grid used by Kazmierczak and Chinoda [16].

The selection of the time step took into account the history of the process, that is the position on the time scale $\tau$, relative to the three phases identified on the right side of Fig. 1. The smallest time step ($\Delta\tau = 0.03$ for the case of Fig. 2) was selected for the start of phase I, in order to capture the steepest gradients that occur in the beginning of this phase (see the detail inserted in Fig. 2). The time step was subsequently increased based on a numerically implemented adaptive time step scheme, which was tested for its accuracy. Relative to leaving the initial time step unchanged throughout phase I, this strategy leads to a reduction in half of the total computational cost for phase I.

For phases II and III, which are dominated by fluctuations caused by the imposed heating, accuracy tests showed that the use of 240 iterations per cycle makes the overall Nusselt number insensitive to further decreases in the time step. In the simulations reported next, the number of iterations per cycle was conservatively set at 400.

The flow and temperature fields of phase I were computed until the steady state was reached. A sample of results for overall Nusselt number ($Nu_c$, $Nu_m$) and average hot wall temperature ($\theta_h$) is presented in Fig. 2. The steady state velocity field ($U$, $V$), pressure field ($P$) and temperature field ($\theta$) were then used as input in the calculation of phases II and III. The calculations were stopped when the steady oscillatory regime was reached, $\tau = \tau_{so}$. The work was done on the IBM 3090

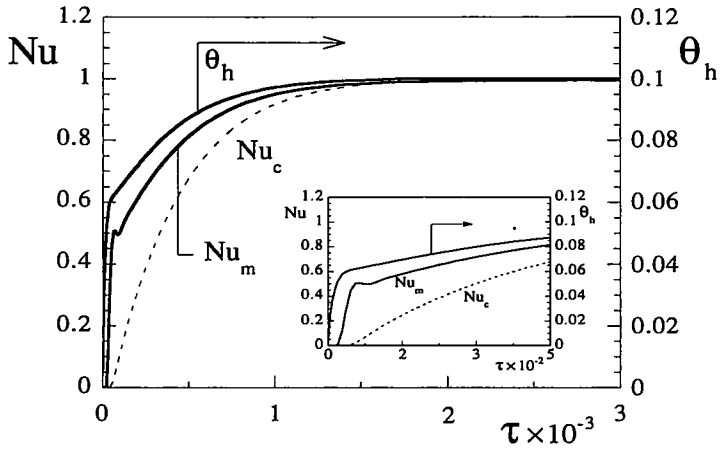


FIG. 2. The behavior of the overall Nusselt numbers and the average hot wall temperature during phase I ($Pr = 7$, $Ra = 10^7$).

at the Cornell National Supercomputer Facility. One run through phases I, II and III required a total CPU time that varied from approximately 2500 s for $Pr = 7$ and $Ra = 10^7$, to approximately 32 000 s for $Pr = 0.01$ and $Ra = 10^7$.

## 4. RESULTS

The strategy of selecting the appropriate ($Pr$, $Ra$) cases for the study of the resonance phenomenon consisted of fixing the Prandtl number and using progressively higher Rayleigh numbers until phase I no longer reaches steady state within a reasonable CPU time. The highest Rayleigh numbers reached in this manner are $Ra = 10^9$ for $Pr = 7$, $Ra = 10^8$ for $Pr = 0.7$, and $Ra = 10^7$ for $Pr = 0.01$. In cases where $Pr = 0.01$ and $Ra > 10^5$, the steady state solution obtained for $Ra = 10^5$ (end of phase I) was used as input for calculating phases II and III. This choice was a trade off between the time required to simulate phase I at high $Ra$ values and the decay time associated with phase II. For each ($Pr$, $Ra$) pair, the frequency $f$ was varied relatively smoothly in order to identify as accurately as possible the wall heat input frequency to which the flow responds in the most visible way.

Figures 3(a)–(c) present an overview of the convection response to changes in frequency and Prandtl number. Each figure corresponds to a single Prandtl number, namely, Fig. 3(a) for $Pr = 7$, Fig. 3(b) for $Pr = 0.7$, and Fig. 3(c) for $Pr = 0.01$. There are three time charts (frames) in each figure, with the imposed frequency $f$ increasing from frame to frame downward. The time scale $\tau$ covers only phases II and III, so that $\tau = 0$ in every frame corresponds to $\tau = \tau_{ss}$ in Fig. 1.

Each frame shows the evolution of four parameters, the cold wall Nusselt number $Nu_c$ (thin solid line), the midplane Nusselt number $Nu_m$ (thick solid line), the imposed heat flux $Q''$ (dash line), and the height-averaged temperature of the hot wall $\theta_h$ (the lowest curve). The middle frames of Figs. 3(a)–(c) correspond to *resonance*, which is defined as the critical frequency $f$ where the amplitude of the $Nu_m$ fluctuation is the greatest.

The results of Figs. 3(a)–(c) have a few additional features in common. In phase III, the fluctuation of $Nu_c$ and $Nu_m$ is nearly sinusoidal even though the imposed heating effect follows a square wave. At frequencies lower than critical (the top frames), the fluctuations of $Nu_m$ and $N_c$ exhibit two frequencies, a primary one, which is the same as the forcing frequency, and a secondary (higher) frequency that is comparable with the critical frequency identified in the next (middle) frame. The instantaneous average temperature of the heated wall has time to reach a locally steady value toward the end of each 'on' or 'off' interval of the imposed heat flux wave $Q''$. This is particularly true at frequencies near or below critical.

Figure 4 shows the instantaneous distribution of heat flux on the cold wall ($Nu_{loc}$) and temperature on the heated wall ($\theta$ at $X = 1$). All the curves are for times $\tau$ that mark the end of one $Q''$ cycle. The fact that the curves come together as $\tau$ increases, is an indication that the flow settles in the steady oscillatory regime (phase III). The upper frame of Fig. 4 is for $Pr = 7$ and corresponds to the run presented in the middle frame of Fig. 3(a). The lower frame of Fig. 4 corresponds to the low Prandtl number simulation that generated the middle frame of Fig. 3(c). Worth noting are the relatively small temperature variations along the heated wall (between 15–30% of the average value $\theta_h$), and that when $Pr = 0.01$ $Nu_{loc}$ is maximum at a height $Y$ of approximately 0.8. This second feature was also noted in an earlier study of low $Pr$ and high $Ra$ convection in a two-dimensional enclosure with isothermal side walls at different temperatures [22].

Figure 5 shows the evolution of the streamline patterns in phases II and III, in an enclosure filled with $Pr = 7$ fluid at $Ra = 10^9$ and $f = 0.018$. This corresponds to the resonance case identified in the middle frame of Fig. 3(a). The streamlines plotted in the first six frames of Fig. 5 represent $\psi$ = constant curves, where the steamfunction $\psi(X, Y, \tau)$ is defined by $U = \partial\psi/\partial Y$ and $V = -\partial\psi/\partial X$, with $\psi = 0$ on the square boundary. Equal increments $\Delta\psi$ separate two adjacent streamlines.

Note further that in Fig. 5 the time $\tau$ increases from left to right, and downward. Each frame that is assembled in the left column corresponds to the end of an 'off' mode of the pulsating heat input, namely, $Q'' = 0.8$ (Fig. 1). The frames placed in the right column are for those instances $\tau$ that mark the end of an 'on' mode, $Q'' = 1.2$. The first four $\psi$ frames are from phase II, while the fifth and sixth (the third row in Fig. 5) illustrate the long-time, periodic and steady behavior (phase III).

This presentation of the evolution of the flow pattern stresses the difference between off and on heating, when seen by the fluid that circulates in the cavity. In the off mode, the cavity fluid decelerates along the heated wall, and returns partially through the core. Note the persistence of two cells (both counterclockwise) in the $\psi$ frames on the left side of Fig. 5. In the on mode, the fluid accelerates along the heated wall, and it is entrained all the way from the opposite (cold wall) boundary layer. The circulation consists of a single counterclockwise cell, which is centered almost in the geometric center of the enclosure in phase III (provided $\tau$ marks the end of the on mode).

The bottom row of Fig. 5 shows the patterns of isotherms in phase III, at the end of the off and on modes. These isotherms correspond to the two frames of streamlines shown in the third row of the same figure. Only two sets of isotherms are shown because their pattern remains practically the same throughout phases II and III. The plot is based on a $\Delta\theta$ increment that remains constant in going from one isotherm to the next. The isotherms show that the vertical walls are always lined by distinct thermal boundary layers,

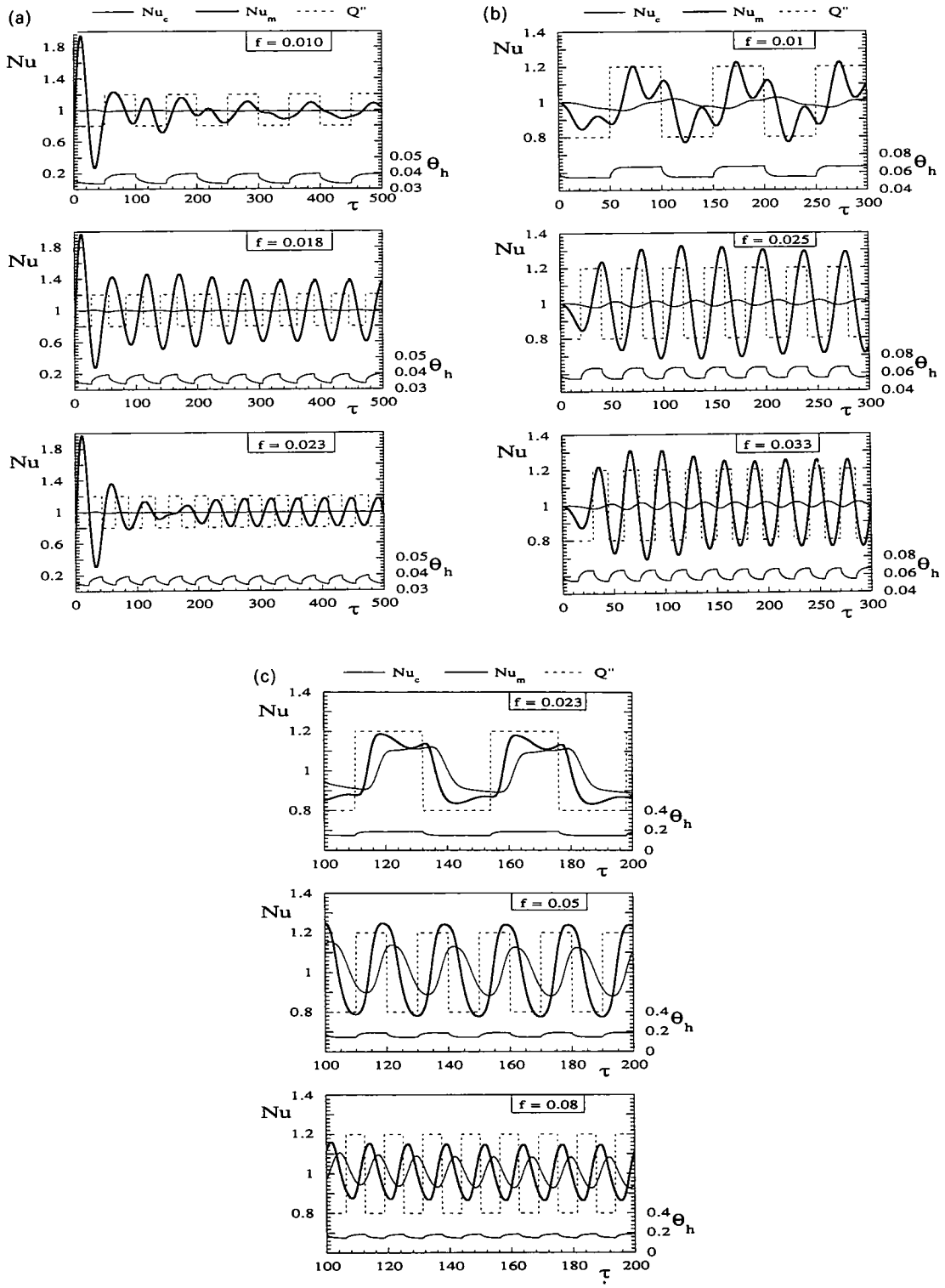


FIG. 3. The behavior of the overall Nusselt numbers and the average hot wall temperature during phases II and III, and the effect of increasing the forcing frequency: (a) $Pr = 7$, $Ra = 10^9$, (b) $Pr = 0.7$, $Ra = 10^8$, (c) $Pr = 0.01$, $Ra = 10^7$.

which are consistent with the boundary layers revealed by the streamline pattern.

The evolution of the flow and temperature fields at low Prandtl numbers is illustrated in Fig. 6, which documents phases II and III of the numerical experiment that also produced the middle frame of Fig. 3(c) (namely, $Pr = 0.01$, $Ra = 10^7$, $f = 0.05$). The flow pattern (the shape of the streamlines) is fairly insen-

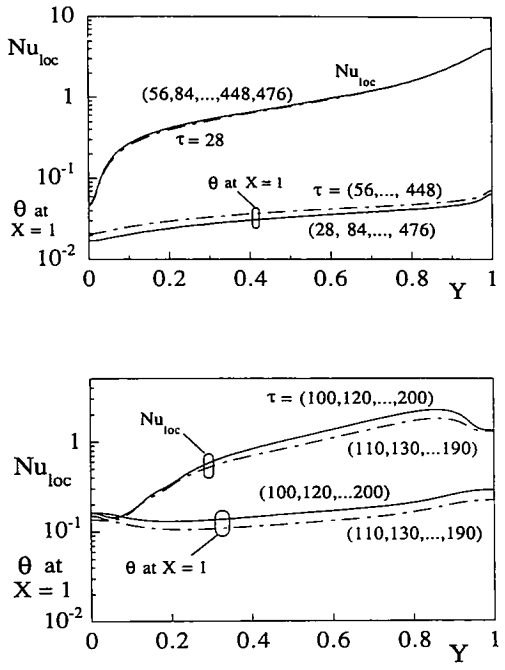


FIG. 4. The cold-wall local Nusselt number and hot wall temperature at the end of each $Q''$ cycle: (top) $Pr = 7$, $Ra = 10^9$, $f = 0.018$, (bottom) $Pr = 0.01$, $Ra = 10^7$, $f = 0.05$.

sitive to the mode of the pulsating heat input, however, the total flowrate (or maximum $\psi$) is 6.07% greater at the end of the on mode than at the end of the off mode. The shape of the isotherms is also insensitive to the mode of the pulsating heat input, provided $\tau$ marks the end of that mode. The thermal boundary layers are distinct ($Ra$ is just high enough), as the spacing between isotherms near the walls is smaller than the spacing in the core region. This feature suggests that convection begins to overtake conduction as the dominant heat transfer mechanism.

The numerical experiments conducted in this part of the study are summarized in Fig. 7. This figure shows the frequency range covered in the search of resonance in the natural circulation, and how the $f$ range depends on the Prandtl number. The value $Nu_{m,max}$ plotted on the ordinate in Fig. 7 is the maximum value of the $Nu_m(\tau)$ wave in the steady oscillatory regime (phase III). Similar maxima are exhibited by the cold-wall Nusselt number curve ($Nu_c(\tau)$, Fig. 3): these are not shown in Fig. 7, because for $Pr \gtrsim 0.7$ the peak value $Nu_{c,max}$ is very close to 1, and the curve $Nu_{c,max}$ vs $f$ would be difficult to see. It is worth mentioning that the existence of resonance is qualitatively similar to the resonance detected by Iwatsu *et al.* [23] in a cavity with thermally stratified fluid, and with an oscillating lid.

Figure 7 shows the resonance effect discussed already in relation to Fig. 3. The curve $Nu_{m,max}$ vs $f$ has a relatively sharp peak at a distinct frequency. The same effect (i.e. peak) is exhibited at the same critical frequency of the $Nu_{c,max}$ vs $f$ curve, which is not shown. The critical frequency determined in this manner appears to be a function of Prandtl number and Rayleigh number. The purpose of the analysis presented in the next section is to derive this function, so that the case-by-case information of Fig. 7 may be extended to regions of the $Pr$ and $Ra$ domains that were not tested numerically.

## 5. SCALE ANALYSIS

One way to explain the fluctuation exhibited by overall quantities such as $Nu_m(\tau)$ and $Nu_c(\tau)$ when $Q''(\tau)$ is imposed, is to consider what happens when the natural circulation (fluid 'wheel' of diameter $\sim H$) completes one turn. The pulsating heat input through the right side of the enclosure paints a sequence of hot and cold spots on the fluid wheel. When these spots cross the vertical midplane and, later, come in contact with the opposite side wall, they induce $Nu_m$ and $Nu_c$ fluctuations that have the same period $w$ as the heat input.

It is reasonable to suspect that the periodicity that the fluid wheel inherits from the heated wall will be accentuated the most when the forcing period $w$ happens to coincide with the period of the wheel rotation,

$$w \sim \frac{4H}{v}. \tag{19}$$

On the right side, $v$ is the scale of the peripheral velocity of the wheel and the product $4H$ represents the wheel perimeter in a square enclosure. The $v$ scale is the same as the scale of the vertical velocity along one of the side walls.

In enclosures containing fluids with Prandtl numbers of order 1 or greater, the vertical velocity scale in the boundary layer is [24]

$$v \sim \frac{\alpha}{H} Ra_{\Delta T}^{1/2} \quad (Pr \gtrsim 1) \tag{20}$$

or, according to equations (15) and (17),

$$v \sim \frac{\alpha}{H} Ra^{1/2} Nu_h^{-1/2} \quad (Pr \gtrsim 1). \tag{21}$$

In boundary layer natural convection due to uniform flux heating from the side, the overall Nusselt number is of the same order as the flux Rayleigh number raised to the one fifth power [24],

$$Nu_h \sim Ra^{1/5} \quad (Pr \gtrsim 1) \tag{22}$$

so that the $v$ scale becomes $(\alpha/H)\, Ra^{2/5}$. This scale and the $f$ definition provided by equations (10, 11) leads to the following estimate for the critical nondimensional frequency represented by the equality of times (19),

$$f \sim \tfrac{1}{4} Ra^{-1/10} Pr^{-1/2} \quad (Pr \gtrsim 1). \tag{23}$$

The dimensional period that corresponds to this $f$ estimate is

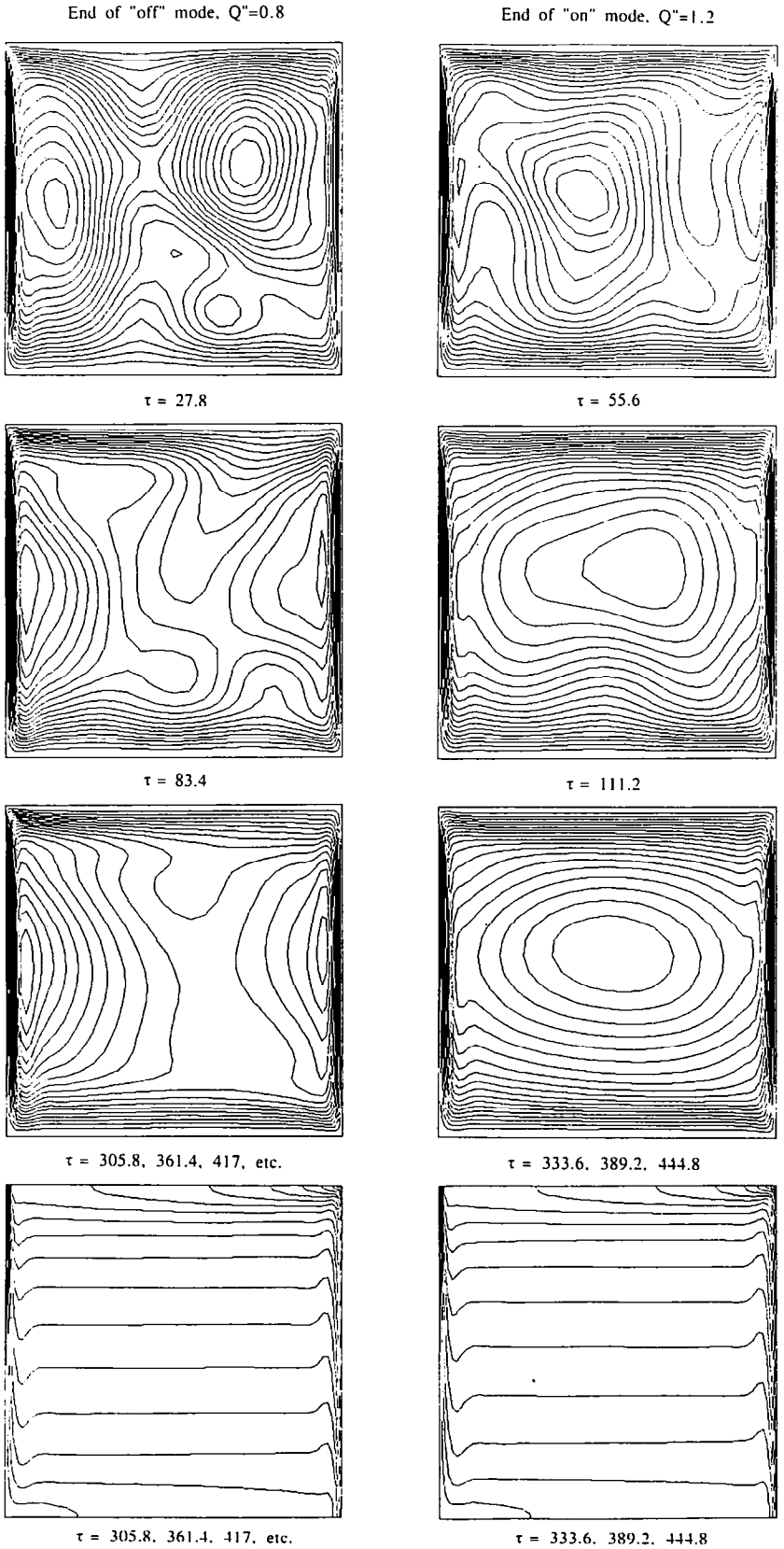


FIG. 5. Streamlines (the top three rows) and isotherms (the bottom row) during phases II and III in a $Pr = 7$ fluid at $Ra = 10^9$ and $f = 0.018$.

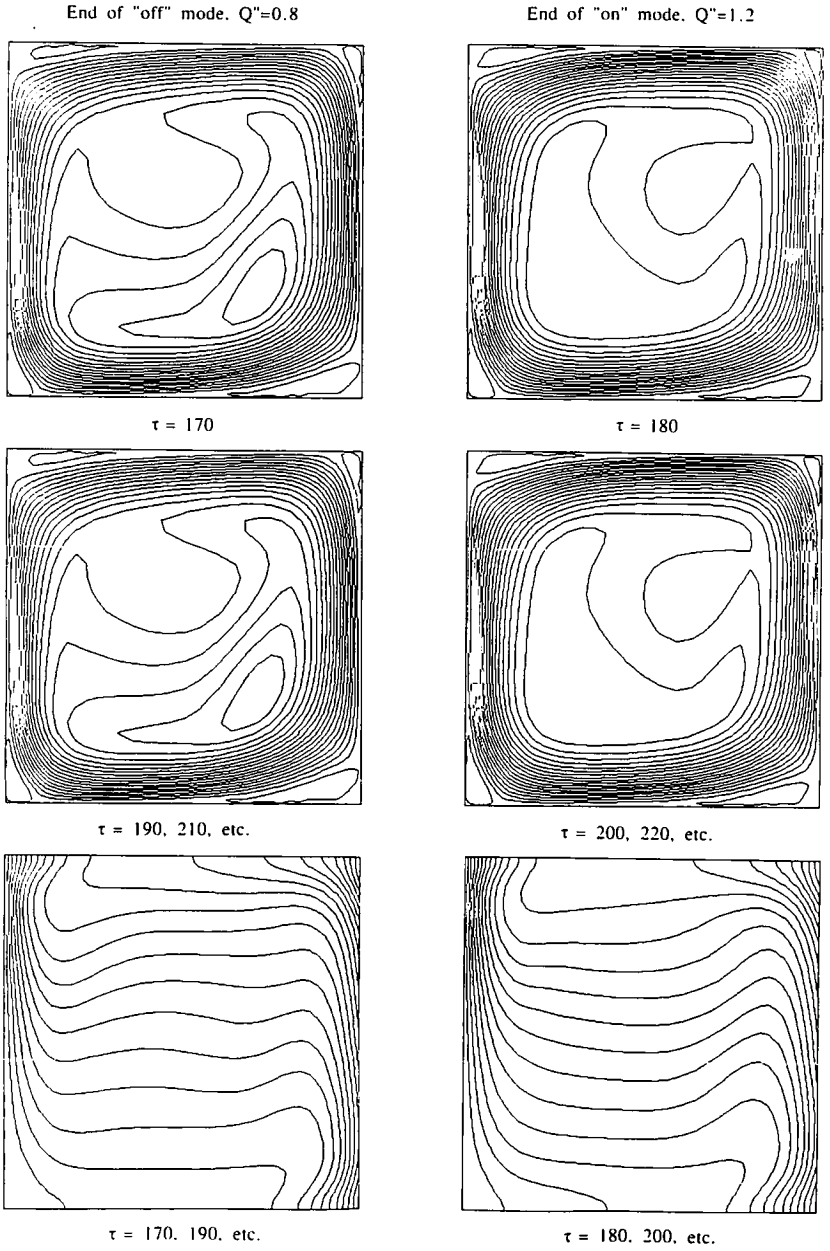


FIG. 6. Streamlines (the top two rows) and isotherms (the bottom row) during phase III in a $Pr = 0.01$ fluid at $Ra = 10^7$ and $f = 0.05$.

$$w \sim 4\frac{H^2}{\alpha} Ra^{-2/5} \quad (Pr \gtrsim 1). \tag{23'}$$

It is worth pointing out that the critical frequency derived in equation (23) is not exactly the same as the Brunt–Väisälä frequency [23, 25], $N \sim (\beta g \Delta T/H)^{1/2}$. If in this $N$ scale we substitute $Nu_h \sim q''_M H/(k\Delta T)$ and, for $Pr \gtrsim 1$, $Nu_h \sim Ra^{1/5}$ (see equation (22)), then the $N$ scale becomes $N \sim Ra^{2/5}(\alpha\nu)^{1/2}/H^2$. In view of equation (10), the nondimensional counterpart of the $N$ frequency is of order $f_N \sim Ra^{-1/10}$, which reproduces only one feature (the $Ra$ dependence) of the critical frequency $f$ identified in equation (23).

This analysis can be repeated for low Prandtl numbers, by assuming that the vertical thermal boundary layers are distinct, which means that [24]

$$(Ra\,Pr)^{1/5} > 1. \tag{24}$$

This condition comes from the statement that the thermal boundary layer thickness ($\sim H(Ra\,Pr)^{-1/5}$) is smaller than the longitudinal length scale ($H$). Note

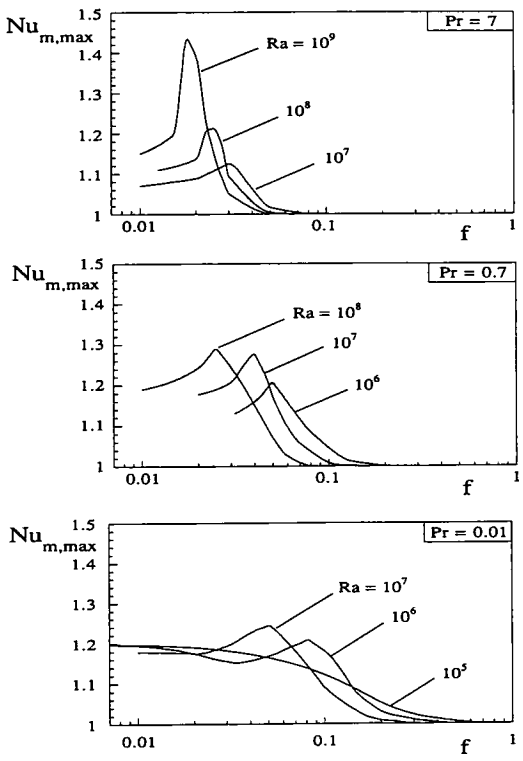


FIG. 7. The effect of the heat input frequency on the maximum of the $Nu_m$ vs $\tau$ wave in the steady oscillatory regime.

that when $Ra = 10^5$ and $Pr = 0.01$, the left side of equation (24) is of order 1, which is why the thermal boundary layers are barely visible (distinct) in the bottom row of Fig. 6. The $Pr < 1$ analysis continues with recognizing the scales

$$v \sim \frac{\alpha}{H}(Pr\, Ra_{\Delta T})^{1/2} \quad (Pr < 1) \tag{25}$$

$$Nu_h \sim (Ra\, Pr)^{1/5} \quad (Pr < 1) \tag{26}$$

and the final results for the nondimensional critical frequency and the corresponding dimensional period are

$$f \sim \tfrac{1}{4}(Ra\, Pr)^{-1/10} \quad (Pr < 1) \tag{27}$$

$$w \sim 4\frac{H^2}{\alpha}(Ra\, Pr)^{-2/5} \quad (Pr < 1). \tag{27'}$$

Table 1 shows a comparison between the critical frequencies determined numerically in Fig. 7, and the theoretical $f$ estimates based on equation (23) or equation (27). The order of magnitude theory performs very well over the entire $Pr$ range considered, provided $Ra$ is high enough so that the vertical boundary layers are distinct. The agreement between the numerical and theoretical values is within 50%.

The theory underestimates the numerical critical frequency when the Prandtl number is large ($Pr = 7$). At $Pr = 0.7$ and $Pr = 0.01$ the theory overestimates the numerical results. When $Ra \leqslant 10^5$ and $Pr = 0.01$, convection is not the dominant heat transfer mechanism (the boundary layers are not distinct) and the $Nu_{m,max}$ vs $f$ curve does not exhibit a sharp peak. The gradual disappearance of the peak as $Ra$ decreases is also evident in the $Pr = 7$ and $Pr = 0.7$ frames of Fig. 7.

## 6. ENCLOSURE FILLED WITH A FLUID SATURATED POROUS MEDIUM

The numerical test presented in Table 1 is also a good opportunity to extend the theory of the preceding section to the realm of natural convection in enclosures filled with fluid saturated porous media. The analogy between natural convection in a pure fluid and natural convection in a fluid saturated porous medium is well known [26, 27]. The only difference is that the square cross-section in Fig. 1 would be filled with a homogeneous porous medium saturated with fluid. The properties of the saturated medium are the thermal diffusivity $\alpha_m$, thermal conductivity $k_m$, Darcy permeability $K$, and the inertia (Forchheimer) coefficient $\chi$. To the definition of $\chi$ we shall return in equation (33).

The critical period of the pulsating heat flux from the side can be estimated based on equation (19), in which $v$ is the scale of the volume averaged vertical velocity. In Darcy flow that scale is [24, 28]

$$v \sim \frac{\alpha_m}{H} Ra_{D,\Delta T} \tag{28}$$

where $Ra_{D,\Delta T}$ is the Darcy modified Rayleigh number based on the average side-to-side temperature difference

$$Ra_{D,\Delta T} = \frac{g\beta KH(\bar{T}_h - T_c)}{\nu\alpha_m}. \tag{29}$$

This Rayleigh number is also equal to $Ra_D/Nu_h$, where $Ra_D$ is the Darcy modified Rayleigh number based on heat flux,

$$Ra_D = \frac{g\beta KH^2 q''_M}{\nu\alpha_m k_m} \tag{30}$$

Table 1. Comparison between the numerical and theoretical estimates for the critical frequency, $f$

| | $Pr = 7$ | | | $Pr = 0.7$ | | | $Pr = 0.01$ | |
|---|---|---|---|---|---|---|---|---|
| | $Ra = 10^7$ | $10^8$ | $10^9$ | $Ra = 10^6$ | $10^7$ | $10^8$ | $Ra = 10^6$ | $10^7$ |
| Numerical, Fig. 7 | 0.030 | 0.025 | 0.018 | 0.05 | 0.04 | 0.025 | 0.08 | 0.047 |
| Theoretical, equations (23) and (27) | 0.019 | 0.015 | 0.012 | 0.07 | 0.05 | 0.04 | 0.10 | 0.08 |

and $Nu_h$ is the overall Nusselt number $q''_M H/k(\bar{T}_h - T_c)$. The $Nu_h$ scale in the distinct boundary layer regime is [24, 29]

$$Nu_h \sim Ra_D^{2/5}. \tag{31}$$

Combining equations (28)–(31), we obtain $v \sim (\alpha_m/H)\, Ra_D^{3/5}$ and the critical period

$$w \sim 4\frac{H^2}{\alpha_m} Ra_D^{-3/5} \quad \text{(Darcy)}. \tag{32}$$

The analysis can be repeated for the inertial, or Forchheimer regime in which the quadratic drag term, $(\chi/v)v^2$, is greater than the Darcy term, $v$, on the left side of the momentum equation for one of the vertical boundary layers [27, 30, 31],

$$v + \frac{\chi}{v}v^2 = \frac{g\beta K}{v}(T - T_{ref}). \tag{33}$$

The units of $\chi$ are [m]. In place of equations (28)–(31) we write, in order,

$$v \sim \frac{\alpha_m}{H} Ra_{F,\Delta T}^{1/2} \tag{34}$$

$$Ra_{F,\Delta T} = \frac{g\beta K H^2(\bar{T}_h - T_c)}{\chi\alpha_m^2} = \frac{Ra_F}{Nu_h} \tag{35}$$

$$Ra_F = \frac{g\beta K H^3 q''_M}{\chi\alpha_m^2 k_m} \tag{36}$$

$$Nu_h \sim Ra_F^{1/5} \tag{37}$$

where $Ra_{F,\Delta T}$ and $Ra_F$ are the Forchheimer modified Rayleigh numbers based on temperature difference and, respectively, average heat flux. The critical period of the pulsating heat input is

$$w \sim 4\frac{H^2}{\alpha_m} Ra_F^{-2/5}. \tag{38}$$

The similarities between the porous medium results (32, 38) and the pure fluid results (23′, 27′) are worth noting.

## 7. CONCLUDING REMARKS

The main conclusion reached in this study is that at sufficiently high Rayleigh numbers where convection is the dominant heat transfer mechanism, the buoyancy driven flow has the tendency to resonate to the periodic heating that is being supplied from the side. The resonance is characterized by maximum fluctuations in $Nu_m$ and $Nu_c$, which physically translate into maximum fluctuations in the local velocity and temperature of the enclosed fluid. It was demonstrated based on numerical experiments that the resonance phenomenon exists in the Prandtl number range 0.01–7, and that it becomes more evident as the Rayleigh number increases.

The numerical results and the order of magnitude analysis showed that the critical period $w$ associated with the resonance phenomenon decreases as the flux Rayleigh number increases, equations (23′) and (27′). The Prandtl number has an effect only if its order of magnitude is lower than 1: the critical period increases as $Pr^{-2/5}$ while $Pr$ decreases, equation (27′). The scale analysis was extended to enclosed porous media saturated with fluid, to predict the critical period that would induce maximum fluctuations in the buoyancy driven flow.

*Acknowledgement*—The numerical work was conducted using the Cornell National Supercomputer Facility, a resource of the Center for Theory and Simulations in Science and Engineering (Cornell Theory Center), which receives major funding from the National Science Foundation and IBM Corporation, with additional support from New York State and members of the Corporate Research Institute. Professor Lage acknowledges with gratitude the support received from the School of Engineering and Applied Sciences of Southern Methodist University.

## REFERENCES

1. D. A. Zumbrunnen, Transient convective heat transfer in planar stagnation flows with time-varying surface heat flux and temperature, *J. Heat Transfer* **114,** 75–93 (1992).
2. J. Patterson and J. Imberger, Unsteady natural convection in a rectangular cavity, *J. Fluid Mech.* **100,** 65–86 (1980).
3. P. Vasseur and L. Robillard, Natural convection in a rectangular cavity with wall temperature decreasing at a uniform rate, *Wärme- und Stoffübertragung* **16,** 199–207 (1982).
4. R. Yewell, D. Poulikakos and A. Bejan, Transient natural convection experiments in shallow enclosures, *J. Heat Transfer* **106,** 533–538 (1983).
5. J. C. Patterson, On the existence of an oscillatory approach to steady natural convection in cavities, *J. Heat Transfer* **106,** 104–108 (1984).
6. G. N. Ivey, Experiments on transient natural convection in a cavity, *J. Fluid Mech.* **144,** 389–401 (1984).
7. T. S. Lee and S. Kauh, Unsteady natural convection in a rectangular enclosure. *Heat Transfer: Korea–U.S.A. Seminar Proceedings*, Department of Mechanical Engineering, Seoul National University, 16–22 October (1986).
8. V. F. Nicolette, K. T. Yang and J. R. Lloyd, Transient cooling by natural convection in a two-dimensional square enclosure, *Int. J. Heat Mass Transfer* **28,** 1721–1732 (1985).
9. J. D. Hall, A. Bejan and J. B. Chaddock, Transient natural convection in a rectangular enclosure with one heated side wall, *Int. J. Heat Fluid Flow* **9,** 396–404 (1988).
10. D. R. Otis, Convection as the dominant mechanism of core stratification during transient natural convection in enclosures at high Rayleigh numbers, *Int. Commun. Heat Mass Transfer* **14,** 597–604 (1987).
11. K. T. Yang, Natural convection in enclosures. In *Handbook of Single-Phase Convective Heat Transfer* (Edited by S. Kakac, R. Shah and W. Aung), Chap. 13. Wiley, New York (1987).
12. S. G. Schladow, J. C. Patterson and R. L. Street, Transient flow in a side-heated cavity at high Rayleigh number: a numerical study, *J. Fluid Mech.* **200,** 121–148 (1989).
13. J. M. Hyun and J. W. Lee, Numerical solutions for transient natural convection in a square cavity with different sidewall temperatures, *Int. J. Heat Fluid Flow* **10,** 146–151 (1989).

14. J. C. Patterson and S. W. Armfield, Transient features of natural convection in a cavity, *J. Fluid Mech.* **219,** 469–497 (1990).
15. S. W. Armfield and J. C. Patterson, Direct simulation of waves interaction in steady natural convection in a cavity, *Int. J. Heat Mass Transfer* **34,** 923–940 (1991).
16. M. Kazmierczak and Z. Chinoda, Buoyancy-driven flow in an enclosure with time periodic boundary conditions, *Int. J. Heat Mass Transfer* **35,** 1507–1518 (1992).
17. J. Mantle, M. Kazmierczak and B. Hiawy, Natural convection in a horizontal enclosure with periodically changing bottom wall temperature, presented at the National Heat Transfer Conference, San Diego, 9–12 Aug. (1992).
18. A. Oberbeck, Ueber die Wärmeleitung der Flüssigkeiten bei Berücksichtigung der Strömungen infolge von Temperaturdifferenzen, *Ann. Phys. Chem.* **7,** 271–292 (1879).
19. J. Boussinesq, *Théorie Analytique de la Chaleur* 2. Gauthier-Villars. Paris (1903).
20. S. V. Patankar, *Numerical Heat Transfer and Fluid Flow*. Hemisphere, Washington, D.C. (1980).
21. R. A. W. M. Henkes and C. J. Hoogendorn, On the stability of the natural convection flow in a square cavity heated from the side, *Appl. Sci. Res.* **47,** 195–220 (1990).
22. J. L. Lage and A. Bejan, The *Ra–Pr* domain of laminar natural convection in an enclosure heated from the side, *Numerical Heat Transfer Part A* **19,** 21–41 (1991).
23. R. Iwatsu, J. M. Hyun and K. Kuwahara, Convection in a differentially-heated square cavity with a torsionally-oscillating lid, *Int. J. Heat Mass Transfer* **35,** 1069–1076 (1992).
24. A. Bejan, *Convection Heat Transfer*. Wiley, New York (1984).
25. J. S. Turner, *Buoyancy Effects in Fluids*. Cambridge University Press, Cambridge, U.K. (1973).
26. S. Kakac, W. Aung and R. Viskanta, *Natural Convection: Fundamentals and Applications*. Hemisphere. Washington, D.C. (1985).
27. D. A. Nield and A. Bejan, *Convection in Porous Media*. Springer-Verlag, New York (1992).
28. D. Poulikakos and A. Bejan, Unsteady natural convection in a porous layer, *Phys. Fluids* **26,** 1183–1191 (1983).
29. A. Bejan, The boundary layer regime in a porous layer with uniform heat flux from the side, *Int. J. Heat Mass Transfer* **26,** 1339–1346 (1983).
30. O. A. Plumb and J. C. Huenefeld, Non-Darcy natural convection from heated surfaces in saturated porous media, *Int. J. Heat Mass Transfer* **24,** 765–768 (1981).
31. A. Bejan and D. Poulikakos, The non-Darcy regime for vertical boundary layer natural convection in a porous medium, *Int. J. Heat Mass Transfer* **27,** 717–722 (1984).